

MSTAR: AN ABSOLUTE METROLOGY SENSOR WITH SUB-MICRON ACCURACY FOR SPACE-BASED APPLICATIONS

Robert D. Peters, Oliver P. Lay, Serge Dubovitsky, Johan P. Burger, Muthu Jeganathan

*Jet Propulsion Laboratory, California Institute of Technology, 4800 Oak Grove Drive, Pasadena CA 91109, USA,
Email: Robert.D.Peters@jpl.nasa.gov*

ABSTRACT

The MSTAR sensor (Modulation Sideband Technology for Absolute Ranging) is a new system for measuring absolute distance, capable of resolving the integer cycle ambiguity of standard interferometers, and making it possible to measure distance with sub-nanometer accuracy. The sensor uses a single laser in conjunction with fast phase modulators and low-frequency detectors. We describe the design of the system - the principle of operation, the metrology source, beam-launching optics, and signal processing - and show results for target distances up to 1 meter. We then demonstrate how the system can be scaled to kilometer-scale distances and used for space-based applications.

1. INTRODUCTION

Space-based applications of precision distance metrology include figure sensing in optical telescopes and radio-frequency antennas, optical pathlength control in stellar interferometers, and precision sensing and formation control of distributed spacecraft instruments and missions. For example, NASA's Space Interferometry Mission (SIM), Terrestrial Planet Finder (TPF) and ESA's Darwin mission all require very precise determination of optical pathlengths within the system. Several large optical telescope designs, currently in the proposal stages, require a sensor for both figure sensing and station keeping of the free-flying telescope elements. For space-based applications, a versatile metrology gauge must be able to operate from a few centimeters to a kilometer. Some applications require the system to produce *unambiguous* range measurements while for others the ability to produce precise unambiguous measurements greatly enhances the metrology system's utility and robustness. The difficulty of producing precise and unambiguous measurements is rooted in the fundamental limitations of laser interferometry, an established method for precision displacement measurement. Nanometer and better precision has been achieved [1,2] with the technique, but absolute distance is ambiguous, because of the inherent half-wavelength ($\sim 0.5 \mu\text{m}$ for a near-IR laser) ambiguity range. To determine the target distance with high accuracy, the ambiguity range of the fine interferometric stage must

be resolved with an additional coarse gauge or gauges. The range accuracy of the coarse stage must be better than the ambiguity range of the relative fine stage; resolving a half-wavelength ambiguity range of $0.5 \mu\text{m}$ requires a 1σ absolute range accuracy of $\sim 0.1 \mu\text{m}$ (peak-valley error $\sim 0.5 \mu\text{m}$), significantly beyond the existing capability.

A number of methods exist for the unambiguous measurement of target distance. The most common method, based on the time-of-flight [3] of emitted pulses, cannot achieve the necessary accuracy, because a timing accuracy of 0.6 femtoseconds is required for a range accuracy of $0.1 \mu\text{m}$. Other techniques, such as intensity-modulated optical beam [4,5], frequency-modulated optical beam, and two-color interferometry [6] are used where higher accuracy is required. The rms accuracy is currently limited to $\sim 5 \mu\text{m}$, although there are examples of higher accuracy in more restricted applications, usually at very short target distances [7-10].

The methods relying on the generation and detection of high-frequency optical carrier modulation suffer from the low responsivity of the high-speed photodetectors required for their operation, and the need for high-speed signal processing electronics.

Two-color interferometry is a technique that avoids the need for high frequency modulation and detection. Two laser interferometer measurements are made at different laser wavelengths. Differencing these measurements is equivalent to having a laser interferometer with a much longer synthetic wavelength [6]. High accuracy over large distances imposes four requirements: (1) the coherence length of the laser must be longer than the round-trip distance to be measured; (2) the laser wavelength must be known to the accuracy needed for the measurement (10 nm accuracy at 100 m requires 10^{-10} wavelength knowledge); (3) the combination of synthetic wavelength and phase resolution must be sufficient to achieve the $0.1 \mu\text{m}$ accuracy; and (4) the synthetic wavelength must be known with high accuracy (0.1 ppm for 1 m distance, 0.01 ppm for 10 m distance, etc.). This combination has not been achieved with existing lasers.

In this paper, we discuss a new architecture that overcomes the existing limitations, and experimentally demonstrate unambiguous measurements with resolution sufficient to resolve the integer cycle ambiguity. The technique, Modulation Sideband Technology for Absolute Ranging (MSTAR), implements a two-color metrology system using a single narrow-linewidth, frequency-stabilized laser; the multiple wavelengths are produced as phase modulation sidebands using fast integrated-optics modulators. This two-color approach avoids the need for the fast photodetectors and signal processing required for other RF modulation schemes [4,5]. The entire system could be implemented with practical space qualifiable components. Another important benefit of the MSTAR system is that the fine relative gauge is an integral part of the system, giving seamless integration of the absolute and fine (sub-nanometer) relative stage into a single high absolute accuracy sensor.

2. THE MSTAR SYSTEM

2.1. Overview

In this section, we summarize the basic MSTAR configuration. The following sections will provide some detail on the different parts of the system.

The system is shown in Fig. 1. The laser light, frequency ν , is split into the Measurement and Local arms. In the Measurement arm the laser frequency is up-shifted by f_M , and a sinusoidal phase modulation $\Delta\Phi \sin(2\pi F_M t)$ is applied, producing a series of sidebands spaced by $\pm F_M, \pm 2F_M, \pm 3F_M, \dots$. Similar modulation, using slightly different frequencies as indicated in Fig. 1, is applied to the Local arm. The resulting optical spectrum for the Measurement and Local beams is shown in Fig. 1b (higher order sidebands have been omitted for clarity). The upper and lower sidebands correspond to the two wavelengths of a two-color interferometer. The electric field amplitude of the k th sideband is given by the appropriate Bessel function: $J_k(\Delta\Phi)$. Weak phase modulation gives a dominant carrier frequency and weak first sidebands. As the modulation level is raised, the sidebands increase in size and number and the carrier level is suppressed. It is also possible to use intensity modulation instead of phase modulation to generate the sidebands; the analysis below will be the same for each case.

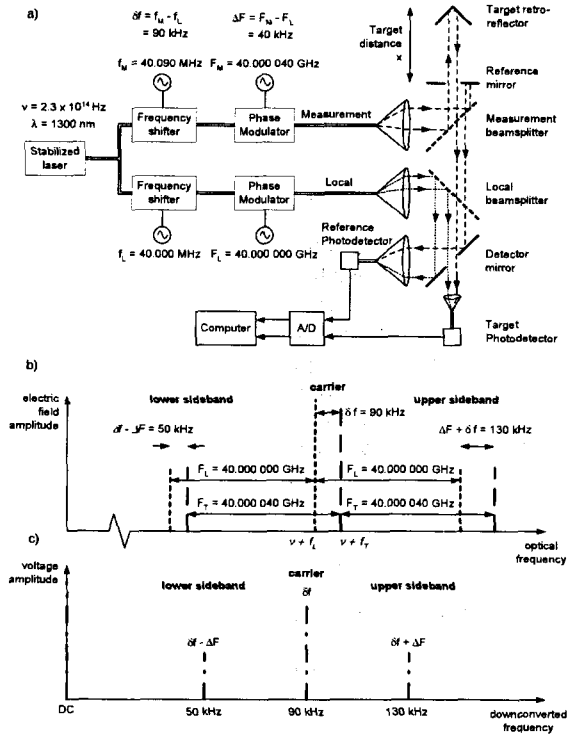


Fig. 1. (a) Schematic of the MSTAR system. The distance to be measured, x , lies between the reference mirror and the target retroreflector. (b) Optical spectrum before photodetection. Long-dashed lines, measurement beams; short-dashed lines, local beams. (c) Spectrum of electrical signals after photodetection.

The Measurement beam is collimated and directed towards the target retroreflector. The outer part of the beam is returned by the Reference mirror. It is attenuated on passing through the Measurement and Local beamsplitters before being deflected to the Reference photodetector. The central core of the Measurement beam propagates to the Target retroreflector, returns through the hole in the Reference mirror and ends up at the Target photodetector. The Local beam takes a shorter route to the two detectors, as shown in Fig. 1a.

The Measurement and Local beams mix at the detectors, generating the down-converted frequencies shown in Fig. 1c (the low-frequency detectors are not sensitive to the high-frequency mixing products between different sidebands). The second sidebands, not shown in Fig. 1c, would be found at 10 kHz and 170 kHz. The choice of modulation frequencies is such that the spectrum at the output of the detectors (Fig. 1c) is a highly compressed version of the optical spectrum (Fig. 1b), with a spacing of 40 kHz instead of 40 GHz.

These low frequency signals greatly simplify the signal processing, and enable the use of much more sensitive low-frequency photodetectors. The photodetector outputs are bandpass filtered to isolate the sinusoids for the carrier, upper, and lower sidebands. The phase difference in cycles (1 cycle = 2π rad) between the carrier sinusoids from the target and reference detectors (each with frequency δf) is given by $\Delta\phi_{car} = (v + f_M)(2x/c)$ where x is the distance between the reflecting surface of the reference mirror and the vertex of the target retroreflector and c is the speed of light.

The integer number of cycles in the phase measurement is unknown and the resulting estimate of x is ambiguous:

$$x_{car} = \frac{c}{2(v + f_M)} (\Delta\phi_{car} \pm m) = L(\Delta\phi_{car} \pm m) \quad (1)$$

where m is an integer. The ambiguity length, L , is half the laser wavelength. The 1σ precision of the length measurement (σ_x) depends on the precision of the phase difference $\sigma_s = L\sigma_{\Delta\phi}$. This type of carrier measurement is similar to that used in a standard heterodyne metrology gauge.

In addition to making this sub-nanometer measurement, MSTAR uses the sidebands added by phase modulation to determine the number of integer cycles m in Eq. 1. The upper and lower sideband phase differences are given by $\Delta\phi_{usb} = (v + F_M + f_M)(2x/c)$ and $\Delta\phi_{lsb} = (v - F_M + f_M)(2x/c)$. Combining these phase differences yield

$$x' = \frac{c}{4F_M} (\Delta\phi_{usb} - \Delta\phi_{lsb} \pm n) = L'(\Delta\phi_{usb} - \Delta\phi_{lsb} \pm n) \quad (2)$$

analogous to Eq. 1 but with a substantially longer ambiguity length, $L' = c/(4F_M)$, and precision $\sigma_{x'} = L'\sqrt{2}\sigma_{\Delta\phi}$. The synthetic wavelength is $c/2F_M$. As an example of how measurement of x' can be used to resolve the ambiguity m , consider the frequencies shown in Fig. 1. The carrier phase ambiguity length is $L = 0.65\mu\text{m}$. With a phase resolution of $\sigma_{\Delta\phi} = 5 \times 10^{-5}$ cycles (0.3 mrad), $\sigma_x = 30\text{pm}$. The sideband combination has $L' = 1.875\text{mm}$ and $\sigma_{x'} = 0.12\mu\text{m}$, sufficient to resolve L (and therefore m) at a high level of probability. We can resolve the remaining ambiguity (n) by switching to a lower phase-modulation frequency. Switching to a phase-modulation frequency of 30 MHz gives $L'' = 2.5\text{m}$ and $\sigma_{x''} = 0.18\text{mm}$, sufficient to resolve n .

2.2. Metrology source

The metrology source includes the stabilized laser, optical fiber, frequency shifters and phase modulators shown in Fig. 1a. The laser is a Nd:YAG system with linewidth of 10 kHz at $1.32\mu\text{m}$, from Lightwave Corporation. The very narrow linewidth has a coherence length of $\sim 30\text{ km}$, which is important for long-range applications. The laser wavelength is measured against a HeNe reference laser using a Burleigh WA-1500 wavemeter (accuracy $\sim 0.1\text{ ppm}$), and a control loop provides feedback to stabilize the laser. The output is coupled into single-mode polarization-maintaining (PM) optical fiber at a level of 200 mW. A fiber splitter sends laser light to the Measurement and Local arms, where the optical frequency is up-shifted by $\sim 40\text{ MHz}$ using acousto-optic modulators, and then fed into high-frequency phase modulators operating at $\sim 40\text{ GHz}$.

The phase modulators are LiNbO₃ devices built by EOSpace. They have a V_π of 5.5 V at low frequency, and a V_π of 11 V at 40 GHz. The phase modulators are driven at $\sim 40\text{ GHz}$ by a pair of Agilent 83650B synthesizers (accurate to $\sim 0.1\text{ ppm}$), with MMIC amplifiers providing an additional 40 dB of gain. With +23 dBm of RF input power, the first sidebands are 13 dB down from the carrier. The modulators have a fiber-to-fiber insertion loss of 3.5dB.

If PM optical fiber is used throughout the metrology source, then the optical path length through the system depends on the polarization state. To avoid this problem, a length of polarizing (PZ) single-mode optical fiber is used between the phase modulators and the collimators, providing a true single polarization mode.

2.3. Beam launcher optics

The MSTAR system described above has 4 paths that the signals should follow, as depicted in Fig. 1a. Light taking any other path to the detectors will cause an error. The phase resolution of $\sigma_{\Delta\phi} = 5 \times 10^{-5}$ cycles (0.3 mrad) requires that the total optical power in the error paths is down by $\sim 70\text{ dB}$ ($20\log_{10}0.0003$). Error paths include multiple back-reflections in a single path, and leakage between the inner and outer parts of the Measurement beam. The beam launcher optics, shown in Fig. 2, were designed to minimize these effects.

The main difference compared to the schematic in Fig. 1a is the addition of polarizing optics to provide a second level of isolation. Light from the Measurement arm passes through a ferrite isolator before collimation, polarizing the light in the s-direction. The isolator suppresses the error path formed by back-reflection

from the Reference mirror followed by back-reflection from the tip of the Measurement collimator. The collimators are 2-inch achromatic doublets. The Measurement beam reflected from the Reference mirror is s-polarized, passing through the Reference Polarizer to the Reference Collimator. Two things prevent this light from reaching the Target collimator: the Target pupil is under-sized compared to the hole in the Reference mirror, and the s-polarization is blocked by the Target polarizer. The inner part of the Measurement beam passes twice through the Target Quarter-Wave Plate, returning as p-polarized light. This light is prevented from reaching the Reference collimator by a combination of the over-sized hole in the Detector mirror, and the Reference polarizer, which does not transit the p-polarization. The Reference and Target Quarter-Wave Plates form isolators with their respective polarizers, and suppress the back-reflections from the fiber tips of the Reference and Target collimators. The Local beam is polarized at a 45-degree angle, so that it couples to both the Target and Reference detectors. The Target retro-reflector is mounted on a manual translation stage, 1 m in length.

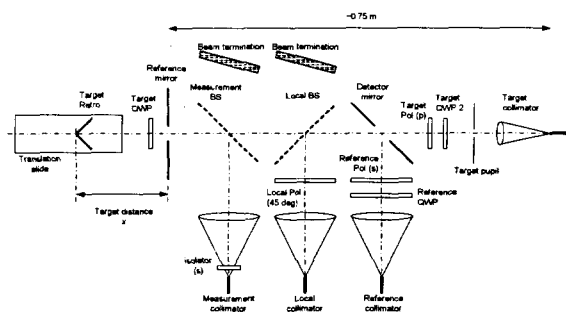


Fig. 2. Beam launcher optics. “s” and “p” indicate the direction of polarization (s is normal to the page, p is in the plane of the page, 45 deg is midway between the two). Pol = Polarizer, QWP = Quarter-Wave Plate.

The current breadboard beam launcher was intended for demonstrating performance in the lab. The use of 2-inch optics and adjustable mounts for most components makes the beam launcher too large to be practical in many applications. The presence of the Target Quarter-Wave Plate in the target path also complicates the measurement of x , since we must correct for the increased electrical length. The next version of the beam launcher will be much smaller, and the use of Angle-Polished fibers may avoid the need for the polarizing optics.

2.4. Signal processing

Achieving a phase resolution of $\sigma_{\Delta\phi} = 5 \times 10^{-5}$ cycles (0.3 mrad) requires some care in the processing of the signals. The detectors are standard battery-operated New Focus 2011 models, which operate up to a bandwidth of 300 kHz and provide switchable levels of gain. The signals are digitized with a Gage 2-channel 14-bit A/D card, sampling at a rate of 500 kHz, such that 2^{16} samples per channel are obtained in a total measurement time of $t_m = 0.13$ s.

The phase as a function of time for each line in the RF spectrum for each detector output is obtained with the following procedure. (1) Each time series is Fourier transformed. (2) The negative frequencies are discarded. (3) For each carrier/sideband in the spectrum, a block of channels centered on the nominal line frequency is extracted. (4) This segment of the spectrum, shifted to DC, is then Fourier transformed to give a complex function in the time domain. The complex argument of this function is the phase of the sideband over the 0.13 s period, $\Delta\phi_k^{(T)}$ or $\Delta\phi_k^{(R)}$. (5) For each carrier/sideband we difference the phases obtained for the Target and Reference detectors, $\Delta\phi_k = \Delta\phi_k^{(T)} - \Delta\phi_k^{(R)}$. The process is essentially a Hilbert transform [11] of the original time series, with additional filtering and down-conversion to isolate the different spectral components, and is much more robust than a zero-crossing approach to phase measurement.

2.5. Verification

In order to verify the accuracy of MSTAR, measurements were compared with a phase meter developed for the Space Interferometry Mission (SIM) [13]. This phase meter, not shown in Fig. 1a, is connected to the outputs of the photodetectors, in parallel with MSTAR data acquisition. It first converts the heterodyne sine wave to square waves to reduce amplitude dependence, then measures the time between the signals on the measurement and reference channel. The phase meter also counts the integer number of cycles to track displacements over large distances.

The MSTAR experiment is run using automatically using the LabView environment. Each measurement with the MSTAR system consists of the following steps:

1. Turn on low-frequency phase modulation with $F_M = 30.040$ MHz and $F_L = 30.000$ MHz
2. Obtain digitized time series simultaneously for the Target and Reference detector outputs and process to give a coarse distance estimate
3. Switch from low-frequency phase modulation to high frequency modulation with $F_M = 40.000,040$ GHz and $F_L = 40.000,000$ GHz

4. Obtain digitized time series simultaneously for the Target and Reference detector outputs and process to give a fine distance estimate
5. Turn off the phase modulation
6. Measure the differential phase with the verification phasemeter
7. Move the target retro-reflector to the desired new position, with the verification phasemeter counting fringes
8. Calculate the change in position from the number of fringe counts from the verification phasemeter. Add this to previous displacements to determine the displacement relative to the original starting position
9. Go to step 1

Note that the MSTAR estimate of the target position is calculated independently at each target position, and the phase modulation is turned off while the target is being moved. When the phase modulation is turned on, the verification phasemeter output is no longer valid – this is why the displacement of the target must be calculated as a sum over a series of steps, each of which is measured with the phase modulation off. The independent “true” position is then given by

$$x_{\text{TRUTH}} = x_{\text{START}} + \sum_i \Delta x_i = x_{\text{START}} + \Delta x_{\text{TRUTH}} \quad (3)$$

where x_{START} is the unknown starting position and Δx_i are the measured lengths of each step.

3. RESULTS

Three types of experiment were conducted to validate performance: (I) a displacement test, (II) a stability test, and (III) a zero test.

(I) *Displacement test.* From an arbitrary starting position the target was moved in small increments along the track. At each position, MSTAR generated a position, x_{MSTAR} , based only on the sideband difference phases. Equation 2 shows that this measurement depends only on the phase modulation frequency (tied to the synthesizer’s frequency reference), and is independent of the laser wavelength. The ‘truth’ measurement depends only on the accuracy of fringe counting by the independent verification phase meter, and the wavelength of the laser light (tied to the wavelength of the HeNe reference laser). An example set of data is shown in Fig. 3, with the MSTAR distance plotted against the ‘truth’. Also shown is the residual, $\sigma'_x = x_{\text{MSTAR}} - \Delta x_{\text{TRUTH}} - x_{\text{START}}$ (note that x_{START} is equated to the first value of x_{MSTAR} , so that $\sigma'_x = 0$ for the first point by definition). The standard deviation of this residual ($0.12 \mu\text{m}$) is typical of the results obtained, and demonstrates that MSTAR can measure *displacements* (as opposed to absolute

position) with the accuracy necessary to resolve the number of integer cycles m .

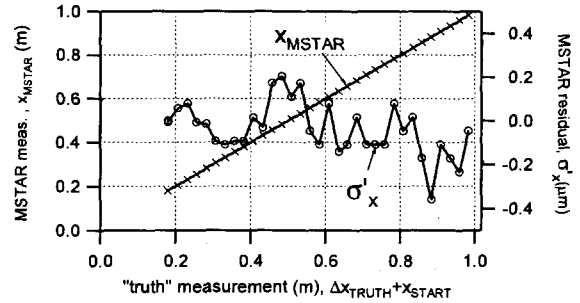


Fig. 3. MSTAR absolute measurement vs ‘true’ displacement from start point (based on fringe counting). The residual error, $\sigma'_x = x_{\text{MSTAR}} - \Delta x_{\text{TRUTH}} - x_{\text{START}}$ is overlaid.

(II) *Stability test.* This test was conducted in the same way as the displacement test, except the target was not deliberately moved (small thermal motions were tracked with the truth measurement). Over a 3-hour period, the standard deviation of the residual was $0.05 \mu\text{m}$, demonstrating that MSTAR is stable and calibratable.

(III) *Zero test.* It was not possible to extend the displacement test down to zero separation between the reference mirror and the vertex of the target retro-reflector. This is because the target retro-reflector and target quarter-wave plate were too large to fit through the small ($\sim 5 \text{ mm}$) hole in the reference mirror (Fig. 3). The annular reference mirror was instead replaced by a standard plane mirror, giving a target surface that is coplanar with the reference. The MSTAR measurements were consistent with zero to within $0.2 \mu\text{m}$.

The tests show that MSTAR’s sideband length estimate measures displacements with accuracy sufficient to resolve the integer-cycle ambiguity. It also measures the absolute zero position correctly. It should be noted that this combination of tests does not rule out the possibility of an anomaly in the MSTAR reading between zero and the start point of the displacement test ($\sim 18 \text{ cm}$). To exclude this possibility, we have replaced the large retro-reflector with a much smaller target retro-reflector that will fit through the hole in the annular reference mirror. A white light interferometer has been put in place to establish when the vertex of the retro-reflector is coincident with surface of the reference mirror. This will establish $x_{\text{START}} = 0$ for the fringe counting verification measurement.

The tests above only address the accuracy of the sideband length estimate (Eq. 2). The MSTAR system simultaneously generates a carrier length estimate (Eq.

1) which, in combination with the sideband length estimate, has subnanometer accuracy. This level of performance was not tested in the experiments.

4. EXTENSION TO SPACE-BASED APPLICATIONS

In the following sections, we address the issues relevant to moving MSTAR from a lab demonstration to a gauge usable for space applications. We cover increasing the range, moving targets and reducing the size of the optics.

4.1. Increased range

The MSTAR system has only been demonstrated in the laboratory for stationary targets, at ranges of up to 1 m. Operation at longer range imposes additional requirements on the system performance:

1. The coherence length of the laser source must be larger than the round-trip optical path to the target.
2. The uncertainty in the laser wavelength must be reduced.
3. The uncertainty in the RF modulation frequency must be reduced in order to resolve the integer cycle ambiguity.
4. The system must accommodate the increased photon noise due to the weaker return signal.
5. The weaker target return signal is more prone to leakage and multi-path effects, requiring increased optical isolation.

Each of these items is addressed below.

4.1.1. Coherence length

As noted in section 2.2, the Lightwave NPRO laser has a linewidth of 10 kHz. The associated coherence length of 30 km is therefore sufficient in principle for target distances of up to 15 km.

4.1.2. Laser wavelength uncertainty

Obtaining range accuracy σ_x at range x , requires knowledge of the laser wavelength to a fraction σ_λ/x . For example, if $x = 100$ m and $\sigma_x = 10$ nm, then the wavelength must be known with fractional uncertainty less than 10^{-10} . High accuracy measurements over long distances will require a frequency stabilized laser source. Since it is the knowledge of the laser frequency that is important, and not just the frequency stability, commonly used Fabry-Perot cavity references cannot be relied upon, since the cavity is prone to long-term drift. Therefore, we must use an atomic or molecular resonant transition as a frequency reference.

The 1.319- μ m wavelength NPRO laser currently used for MSTAR has a frequency of 2.3×10^{14} Hz. In order

to achieve a position uncertainty of 10 nm over a target separation of 100 m, we must know the laser frequency to within 23 kHz. We have investigated a variety of frequency standards and locking techniques that could achieve this level of frequency accuracy. We believe the best frequency standards for MSTAR would be either molecular iodine or methane. Methane may be used directly with the laser wavelength of 1.319 μ m, whereas iodine would require the laser frequency to be doubled to give a wavelength of 659 nm.

Locking a doubled 1319 nm laser to iodine has already been demonstrated [14] with frequency uncertainty of 2.4×10^{-10} (55 kHz). The frequency stabilization system locks on the Lamb-dip [15] at the center of the Doppler broadened absorption profile, using an FM spectroscopy technique similar to that used in common Pound-Drever-Hall [16] locking systems. We believe that similar performance may be achieved using methane without the need for frequency doubling.

4.1.3. Modulation frequency uncertainty

Resolving the integer-cycle ambiguity requires a range resolution of ~ 100 nm for the sideband length estimate. The phase modulation frequency must therefore be known with fractional uncertainty less than $(100 \text{ nm} / x)$. For $x = 100$ m, the knowledge requirement is 10^{-9} , which is easily met by a number of frequency standards [17]. Compact Rubidium-based systems have an accuracy of $\sim 5 \times 10^{-11}$; laser-cooled Cesium systems approach 10^{-15} .

4.1.4. Increased photon noise

As the photon rate for the return signal is reduced, shot noise becomes the dominant source of random noise in the system. The photon rate can be increased by using a higher power laser, or by increasing the diameter of the target beam and retro-reflector to minimize diffraction losses. This is not necessary, however, since the coherent integration time can be increased arbitrarily, even in the presence of vibration and target motion, using the carrier-aided smoothing technique (section 4.2).

4.1.5. Increased leakage

The weaker return signal is also more susceptible to multi-path effects and leakage from the reference part of the beam (section 2.3). Higher laser power and longer integration times are not going to help with this systematic error. In the far-field limit, the optical return loss for the target beam is proportional to d^4 , where d is the outgoing beam diameter. A large target beam is therefore highly advantageous. The isolation properties of the beam launcher are also likely to be improved by going to a more compact design that minimizes the

effects of diffraction, and uses angle-polished fibers to minimize back-reflections.

4.2. Moving targets

The discussion and analysis up to this point has assumed that the length being measured is constant over the duration of the measurement time. As the range is increased, the returned signal power goes down, and longer coherent integration times are required to resolve the integer cycle ambiguity. The requirement of no motion over this interval then becomes restrictive for many applications; for example, large structures are liable to bend and flex, and optics distributed over multiple spacecraft may exhibit large relative motions.

Fortunately, MSTAR is able to overcome this problem using a technique called 'Carrier-Aided Smoothing', first developed for Global Positioning System applications [12]. The MSTAR sensor generates two estimates of the distance: the carrier length estimate based on the optical phase of the carrier frequency, and the sideband length estimate based on the phase difference between the sidebands. The carrier length estimate gives the change in range over the measurement time, relative to the starting value, precise to the nanometer level. This range vs time can then be subtracted off the time series generated by the sideband length estimate. Having removed the effects of motion, we can average the sideband length estimate coherently over an arbitrarily long time interval to increase the signal-to-noise ratio. The result obtained gives the absolute range for the start of measurement time interval, which can be combined with the time series of the carrier length estimate to give an absolute measurement of the range as a function of time.

4.3. Smaller optics

As was stated in section 2.3, the current MSTAR beam launcher is a tabletop unit assembled with mostly off the shelf optics and mounts. Consequently it is rather bulky and occupies 3 ft x 2 ft x 2 ft. Space applications require the beam launcher to be lightweight, extremely compact and rugged. We plan to build a custom opto-mechanical beam launcher similar to those developed for the Space interferometry Mission (SIM) [2]. With tight opto-mechanical integration, the launcher could be the size of a thick book (size of 25cm x 15cm x 6cm). These passive beam launchers will be linked by fibers to the source and detection electronics. A reference plane will be provided on the launcher to function as a zero for the measurement beam. Substantial further reduction in size and weight may be possible if we can minimize the internal beam size while maintaining the high isolation between the local and target beams in the presence of diffraction effects.

In summary, we do not believe there are serious obstacles to scaling the performance of MSTAR to ranges of 100 m or more. Additionally, a smaller integrated launcher package and modifications to the signal processing will allow MSTAR to be scaled to space applications.

5. SPACE-BASED APPLICATIONS

The MSTAR system could be very useful in space-based applications such as stellar interferometry, distributed spacecraft control and figuring of optical telescopes and radio-frequency antennas. Here we will provide a brief example of how MSTAR could provide a benefit over existing systems.

5.1. Interferometry

Interferometers require precision optical pathlength control to balance the optical paths in each arm of the interferometer. Traditionally, this pathlength control has been accomplished with heterodyne metrology gauges. However, these systems suffer from drawback if there is an interruption of the metrology gauge, or if a motion exceeds the bandwidth of the phasemeter. Any measurement made after such a condition may be off by many fringe counts. The system may then need to go through a recalibration process by moving back to a "home" position and then resume tracking with the metrology. With an absolute metrology system such as MSTAR, an interruption of this type is easily recovered from without the need of recalibration.

5.2. Figure sensing

High performance optical telescopes and radio-frequency antennas may require careful monitoring of the shape of their primary reflectors. While instruments exist to easily measure surface figure of objects in the lab, they do not lend themselves to an active monitoring of an object in space. Although the MSTAR gauge presented here is a single axis linear gauge, careful engineering could combine multiple gauges to measure key locations of a surface and actively monitor the figure.

Another option would be to scan a single MSTAR gauge to multiple targets. In this situation, the surface resolution could be much higher than what might be allowed by the space and weight of multiple gauges. The trade-off is the time that it takes to scan through the number of target locations on the surface to obtain the desired resolution.

6. SUMMARY

We have described the architecture and operation of the MSTAR sensor; a new distance-measuring system

based on the use of fast phase modulators. The target modulator generates carrier sidebands – the multiple ‘colors’ of an absolute metrology system – which are down-converted by the sidebands produced by the local modulator, enabling low-speed detection and signal processing. The beam-launcher is optimized to minimize cross-talk and leakage between the beams, so that we can measure phase differences with an accuracy of 0.3 mrad. The combination of high-speed modulation (40 GHz) and high phase resolution lead to an absolute range resolution of ~100 nm, sufficient to resolve the integer cycle ambiguity of standard laser metrology systems (also an integral part of the MSTAR sensor), and making possible long-range distance measurement with unprecedented accuracy. Although MSTAR has only been demonstrated over distances of up to 1 m, we show that there are no major obstacles to achieving sub-micron performance over much longer ranges with a much smaller footprint for space applications.

The work described in this paper was performed at the Jet Propulsion Laboratory, California Institute of Technology, under contract with the National Aeronautics and Space Administration.

7. REFERENCES

1. N. Bobroff, *Recent advances in displacement measuring interferometry*, Meas. Sci. Technol., vol. 4, pp. 907-926, 1993.
2. F. Zhao, *Demonstration of sub-Angstrom cyclic non-linearity using wavefront-division sampling with a common-path laser heterodyne interferometer*, American Society of Precision Engineering Annual Meeting, Arlington, VA, Nov 10-15 (2001)
3. O. Bock, *Relative positioning precision of the wide-angle airborne laser ranging system*, J. Opt. A, vol. 1, pp. 77-82, 1999.
4. I. Fujima, S. Iwasaki, and K. Seta, *High-resolution distance meter using optical intensity modulation at 28 GHz*, Meas. Sci. Technol., vol. 9, pp. 1049-1052, 1998.
5. J. M. Payne, D. Parker, and R. G. Bradley, *Range-finder with fast multiple range capability*, Rev. Sci. Inst., vol. 63, pp. 3311-3316, 1992.
6. R. Dandliker, R. Tharman, and D. Prongue, *Two-wavelength laser interferometry using super-heterodyne detection*, Opt. Lett., vol. 13, pp. 339-343, 1988.
7. J. A. Stone, A. Stejskal, and L. Howard, *Diode lasers in length metrology: application to absolute distance interferometry*, Cal Lab, 1999.
8. D. Xiaoli and S. Katuo, *High-accuracy absolute distance measurement by means of wavelength scanning heterodyne interferometry*, Meas. Sci. Technol., vol. 9, pp. 1031-1035, 1998.
9. P. de Groot, *Three-color laser-diode interferometer*, Appl. Opt., vol. 30, pp. 3612-3616, 1991.
10. C. C. Williams and H. K. Wickramasinghe, *Absolute optical ranging with 200-nm resolution*, Opt. Lett., vol. 14, pp. 542-544, 1989.
11. R. N. Bracewell, *The Fourier Transform and its applications*, McGraw-Hill, New York, 1986.
12. R. Hatch, *The Synergism of GPS Code and Carrier Measurements*, Proceedings of 3rd International Geodetic Symposium on Satellite Doppler Positioning, DMA/NGS, pp. 1213-1232, Washington, D.C. (1982)
13. P. Halverson, D. Johnson, A. Kuhnert, S. Shaklan, R. Spero, *A multichannel averaging phasemeter for picometer precision laser metrology*, Proc. SPIE, **3740**, 646-649 (1999).
14. A. Arie, M. L. Bortz, M. M. Fejer and R. L. Byer, *Iodine spectroscopy and absolute frequency stabilization with the second harmonic of the 1319-nm Nd:YAG laser*, Opt. Lett., **18**, 1757-1759, (1993)
15. V. S. LevTokov, *Saturation spectroscopy in high resolution laser spectroscopy*, Topics in Applied Physics, **16** 849 (1991).
16. R.W.P. Drever, J. L. Hall, F. V. Kowalski, J. Hough, G. M. Ford, A. J. Munley, and H. Ward, *Laser Phase and Frequency Stabilization Using an Optical Resonator*, Appl. Phys. B, **31**, 97 (1983).
17. National Institute of Standards and Technology website, Time and Frequency division, <http://www.boulder.nist.gov/timefreq/>